High-Mobility Few-Layer Graphene Field Effect Transistors Fabricated on Epitaxial Ferroelectric Gate Oxides

X. Hong,[1] A. Posadas,[2] K. Zou,[1] C. H. Ahn,[2] and J. Zhu[1]
[1]*Department of Physics, The Pennsylvania State University, University Park, Pennsylvania 16802, USA*
[2]*Department of Applied Physics, Yale University, New Haven, Connecticut 06520, USA*
(Received 17 September 2008; published 2 April 2009)

The carrier mobility μ of few-layer graphene (FLG) field-effect transistors increases tenfold when the SiO_2 substrate is replaced by single-crystal epitaxial $Pb(Zr_{0.2}Ti_{0.8})O_3$ (PZT). In the electron-only regime of the FLG, μ reaches 7×10^4 $cm^2/V\,s$ at 300 K for $n = 2.4 \times 10^{12}/cm^2$, 70% of the intrinsic limit set by longitudinal acoustic (LA) phonons; it increases to 1.4×10^5 $cm^2/V\,s$ at low temperature. The temperature-dependent resistivity $\rho(T)$ reveals a clear signature of LA phonon scattering, yielding a deformation potential $D = 7.8 \pm 0.5$ eV.

DOI: 10.1103/PhysRevLett.102.136808 PACS numbers: 73.50.−h, 72.10.−d, 77.84.Dy

Recent calculations show that the intrinsic mobility of graphene, set by longitudinal acoustic (LA) phonon scattering, can reach $\sim 10^5$ $cm^2/V\,s$ at room temperature [1]. However, extrinsic scattering sources, many of which arise from the surface morphology, chemistry, structural, and electronic properties of the widely used SiO_2 substrate, limit the mobility to the current range of $2 \times 10^3 - 2 \times 10^4$ $cm^2/V\,s$ [1–11]. Increasing the mobility beyond the extrinsic limits is one of the central challenges of the graphene community. Recently, two groups have reported a significant improvement in the mobility of suspended graphene after current-heating annealing [12,13]. A more device friendly solution involves placing graphene on a different substrate. Several alternatives have been explored although they result in graphene mobilities comparable to that on SiO_2 [14].

In this Letter, we report significant carrier mobility improvement in few-layer graphene (FLG) field-effect transistors (FETs) fabricated with single-crystal epitaxial $Pb(Zr_{0.2}Ti_{0.8})O_3$ (PZT) films as the gate oxide. At 300 K, PZT-gated FLG exhibits a mobility $\mu \sim 7 \times 10^4$ $cm^2/V\,s$ at a density of $n = 2.4 \times 10^{12}/cm^2$, reaching 70% of the intrinsic limit set by LA phonons. We observe a clear signature of LA phonon scattering in the temperature dependence of resistivity $\rho(T)$. The PZT-gated FLG shows a residual resistivity ρ_0 at low temperature approximately an order of magnitude lower than that of SiO_2-gated single and few-layer graphene. This low ρ_0 corresponds to $\mu = 1.4 \times 10^5$ $cm^2/V\,s$ and a long carrier mean free path of 2 μm at $n = 2.4 \times 10^{12}/cm^2$. Our results open up a promising route into realizing graphene's full scientific and technological potential [3,15].

FLG flakes are mechanically exfoliated from Kish graphite onto 400 nm, crystalline PZT films epitaxially grown on Nb-doped single-crystal $SrTiO_3$ (STO) substrates via radio-frequency magnetron sputtering [16]. Details are given in Ref. [17]. Figure 1(a) shows the optical and atomic force microscopy (AFM) images of a FLG on PZT. FETs are made by conventional lithography in the Hall-bar geometry. The Nb-doped STO substrate serves as the backgate to which a bias voltage V_g is applied to tune the carrier density of the FLG [Figs. 1(b) and 1(c)]. Results reported here are collected from 3 FETs fabricated on the same PZT substrate and one FET on a SiO_2 substrate.

Resistivity and Hall measurements were performed in a ^{4}He cryostat with a base temperature of 1.4 K, equipped with a superconducting magnet. Standard low-frequency (47 Hz) lock-in techniques are used with excitation currents ranging from 50 to 200 nA. In Fig. 2, we show the sheet resistivity ρ of a 2.4 nm FLG [Fig. 1(c)] as a function of V_g at temperatures 4 K $< T <$ 300 K. $\rho(V_g)$ displays a broad maximum at the charge neutrality point (CNP). Curves below 300 K are shifted to align the $\rho(V_g)$ maximum at $V_g = 0$ V [18]. FLG of this thickness behaves as a

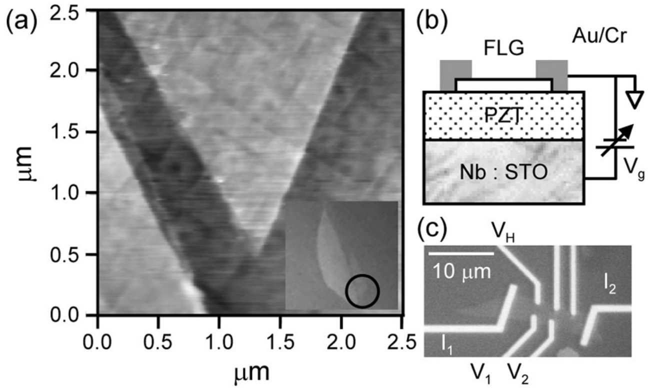

FIG. 1. AFM contact mode image of a 2.4 nm FLG flake (center) on a 400 nm PZT film. Inset: optical image of the whole flake with the area in (a) circled. The PZT surface shows smooth terraces separated by *a*-axis lines, with a root-mean-square (rms) surface roughness of 3–4 Å over a 1 μm^2 area. FLG has a roughness of 2–3 Å. (b) Device schematics. (c) Hall bar configuration of a FLG-FET with current (I_1, I_2) and voltage electrodes for resistance (V_1 and V_2) and Hall (V_1 and V_H) measurements. We determine the thickness of this FLG to be (2.4 ± 0.3) nm based on its optical transparency.

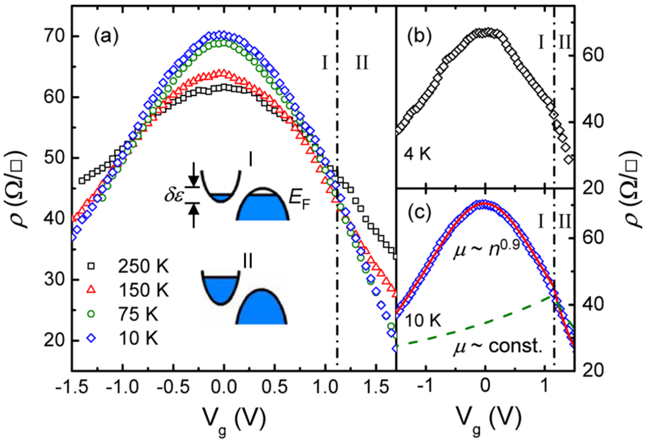

FIG. 2 (color online). (a) $\rho(V_g)$ at selected temperatures taken on the device shown in Fig. 1(c). Inset: schematics of the band structure of FLG of this thickness. (b) $\rho(V_g)$ at 4 K. The kink at $V_g^T = 1.1$ V (dash-dotted line) marks the boundary between regimes I and II. (c) $\rho(V_g)$ at 10 K (open symbols) with a fitting curve (solid line) combining Eqs. (1) and (3) with $\beta = 0.9$ and $r = 0.6$. The dashed line is calculated from Eq. (1) assuming a density-independent mobility $\mu_e = \mu_h = 1 \times 10^5$ cm^2/V s.

two-dimensional (2D) semimetal, where the low-energy bands for electrons and holes are parabolic and overlap slightly [19] [inset of Fig. 2(a)]. The carrier density in the FLG is controlled by V_g through n_e-$n_h = \alpha V_g$, where α is the charge injection rate of the backgate. In the band-overlap regime [regime I in Fig. 2(a) inset], both electrons and holes contribute to conduction:

$$\frac{1}{\rho} = e(n_e\mu_e + n_h\mu_h). \tag{1}$$

At sufficiently large $|V_g|$, the system becomes a pure 2D electron [regime II in Fig. 2(a) inset] or hole (not shown) gas [19]. There, the resistivity and the Hall coefficient R_H are given by

$$\frac{1}{\rho} = en_{e,h}\mu_{e,h}; \qquad R_H = \frac{1}{en_{e,h}}; \qquad n_{e,h} = \alpha V_g. \tag{2}$$

We measure R_H in the hole-only regime of two devices and determine $\alpha = 1.35 \times 10^{12}$ cm^{-2}/V. Using a parallel-plate capacitor model, we extract a dielectric constant $\kappa \approx 100$ for our PZT films. This value is confirmed by independent low-frequency capacitance measurements [17]. The high κ enables PZT to efficiently inject carriers into graphene and screen the effect of charged impurities.

It is clear from Eqs. (1) and (2) that $\rho(V_g)$ changes slope at a threshold V_g^T, where the sample transitions from a two-carrier to a single-carrier regime. Indeed, a kink at $V_g^T = 1.1$ V is clearly visible in $\rho(V_g)$ at low temperature [Fig. 2(b)], where $n_e = 1.5 \times 10^{12}$/cm^2 and $n_h = 0$. Modeling the FLG in regime I with one electron and one hole band and using the effective mass values determined in Ref. [19] for this thickness ($m_e^* = 0.06m_0$ and $m_h^* = 0.10m_0$), we estimate the electron and hole densities at the CNP to be $n_e^0 = n_h^0 \sim 9 \times 10^{11}$/cm^2. This corresponds to an overlap between the electron and hole bands of ~30 meV (see Ref. [17] for more discussions). These estimates are in good agreement with results obtained using methods described previously [19] and band structure calculations of FLG of this thickness [20]. These studies also suggest that FLG in this thickness range may have more than one hole band [19,20]. We emphasize that the central results of the present study are obtained in the electron-only regime described by Eq. (2), and do not rely on the accurate knowledge of the band structure in the two-carrier or hole-only regimes.

In single and few-layer graphene prepared on SiO$_2$ substrates, the mobility is found to be roughly n-independent [6,7,19]. $\rho(V_g)$ calculated using Eq. (1) and a constant μ is plotted in Fig. 2(c) (dashed curve). This curve clearly does not describe our data (open symbols) in the band-overlap regime (I). Instead, a density-dependent mobility $\mu_{e,h} \sim n_{e,h}^\beta$ produces an excellent fit to the data within the entire regime. The power-law functional form is motivated by measurements in regime II, shown later. The solid line in Fig. 2(c) shows such fitting with mobilities determined by

$$\mu_e(n_e) = cn_e^\beta; \qquad \mu_h(n_h) = crn_h^\beta \tag{3}$$

where we require μ_e and μ_h to have a power-law dependence on n_e and n_h, respectively, with the same exponent β but scale by a factor r. We obtain $\beta = 0.9$ from the fit in Fig. 2(c) (see Ref. [17] for other fitting scenarios). The constant c is determined by matching a measured data point $\mu_e = 1.0 \times 10^5$ cm^2/V s at the electron density of $n = 1.75 \times 10^{12}$/cm^2 in regime II. The approximate symmetric V_g-dependence $\rho(V_g)$ displayed for both carriers in regime I, together with $\beta \sim 1$, implies that $r = \frac{\mu_h(n_h)}{\mu_e(n_e)} \sim m_e^*/m_h^* \sim 0.6$. In Ref. [17], we show that the above fitting parameters $r = \frac{\mu_h(n_h)}{\mu_e(n_e)} = 0.6$ and $\beta = 0.9$ also describe the slope and offset of the $R_H(V_g)$ data in the vicinity of the CNP very well. Large e-h asymmetry in μ has been observed in graphene samples [11,12]. Its origin is unclear at the moment.

The above analysis provides an approximate scenario of transport in the two-carrier regime of the FLG. Below, we present and analyze the central results of our work, derived from data taken in regime (II) of the FLG ($V_g^T > 1.1$ V), where the FLG behaves as a one- band, purely 2D electron gas described by Eq. (2). Figure 3 plots $\rho(T)$ extracted from data shown in Fig. 2(a) at five electron densities ranging from 1.9×10^{12}/cm^2 (at $V_g = 1.4$ V) to 2.4×10^{12}/cm^2 (at $V_g = 1.8$ V), well into regime II. At a fixed n, $\rho(T)$ follows a linear T-dependence between 100 and 300 K and quickly saturates to a nonzero residual value $\rho_0(n)$ at lower T. This linear T-dependence, its temperature range, and the magnitude of the resistivity change strongly point to scattering between electrons and LA phonons in graphene. Indeed, in a 2.4 nm FLG, both

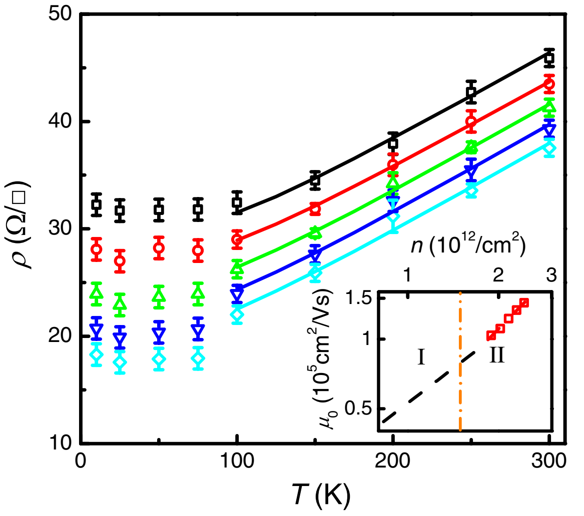

FIG. 3 (color online). $\rho(T)$ at electron densities of (from top to bottom) $n = 1.89$, 2.02, 2.16, 2.30, and $2.43 \times 10^{12}/\mathrm{cm}^2$. The solid lines are fittings to Eq. (4) for $T > 100$ K, with the corrections due to a nondegenerate Fermi gas included. Inset: Low-T residual mobility $\mu_0(n)$ in a double-log plot. Open squares are data taken in regime II. The dashed line plots the fitting [Eq. (3), electrons] obtained in regime I.

electrons and phonons are two-dimensional. The resistance due to LA phonon scattering has been calculated [1] and experimentally studied [10] recently in graphene on SiO$_2$. However, the combination of a large ρ_0 and the onset of another scattering mechanism at 150 K in SiO$_2$-gated graphene makes it difficult to extract the LA phonon contribution unambiguously in those systems [10].

In our devices, a small ρ_0 enables us to clearly observe the predicted linear T-dependence at $T > T_{\mathrm{BG}}$, where $T_{\mathrm{BG}} = \frac{2\hbar k_F v_{ph}}{k_B} \approx 80$ K is the Bloch-Gruneisen temperature at $n = 2 \times 10^{12}/\mathrm{cm}^2$, using a sound velocity $v_{\mathrm{ph}} = 2.1 \times 10^6$ cm/s for LA phonons in graphene and $k_F = \sqrt{\pi n}$ for the Fermi wave vector of the 2D electron gas. At $T > T_{\mathrm{BG}}$, the contribution to the resistivity from LA phonons is given by

$$\rho_{\mathrm{ph}}(T, n) = \frac{m_e^*}{ne^2}\left\langle\frac{1}{\tau}\right\rangle = \frac{1}{n}\frac{(m_e^*)^2 D^2 k_B T}{4\hbar^3 e^2 \rho_m v_{\mathrm{ph}}^2} \qquad (4)$$

where we have modified the derivation in Ref. [1] to account for massive electrons in FLG. D is the unscreened acoustic deformation potential [17] and $\rho_m = 6.5 \times 10^{-7}$ kg/m^2 is the areal mass density of graphene. The correction due to a nondegenerate Fermi gas is less than a few percent in our density and temperature range and is neglected in Eq. (4). Solid lines in Fig. 3 show fittings at different densities for $T > 100$ K, where the slopes range from 83 to 87 mΩ/K and lead to $D = 7.8 \pm 0.5$ eV in graphene. This result falls within the range of reported values in the literature of 1–30 eV [10,21–24] and agrees very well with tight-binding calculations producing $D \sim 3\gamma$, where $\gamma \sim 3$ eV is the nearest-neighbor hopping matrix [22]. We do not observe evidence of superlinear T-dependences reported in graphene on SiO$_2$ [7,10] that are attributed to remote substrate [9,10] or inter-ripple flexural phonons [7]. We speculate that a higher stiffness and a larger average carrier-substrate separation in FLG may be responsible for suppressing scatterings from these two types of phonons.

The small residual resistivity ρ_0 in PZT-gated FLG leads to mobility μ_0 in excess of 1×10^5 cm^2/V s at low T. Since both FLG and single-layer graphene are subject to similar scattering mechanisms, a comparison between μ of PZT-gated FLG, SiO$_2$-gated FLG, and SiO$_2$-gated graphene highlights the important role played by the substrate. Such comparison is shown in Fig. 4, where we compare $\mu(T)$ obtained from two 2.4 nm thick FLG (one on PZT, one on SiO$_2$ [17]), graphene on SiO$_2$ from Ref. [10], bulk graphite from Ref. [21] and the intrinsic LA phonon-limited mobility calculated from Eq. (4), using $D = 8$ eV. At a density of $n = 2.4 \times 10^{12}/\mathrm{cm}^2$, the PZT-gated device shows $\mu \sim 7 \times 10^4$ cm^2/V s at room temperature, 70% of the intrinsic phonon mobility of $\sim 1 \times 10^5$ cm^2/V s. At low T, μ increases to 1.4×10^5 cm^2/V s, corresponding to a long mean free path of 2 μm. A second device ($\sim$5 nm thick, not shown) on the same PZT substrate exhibits mobilities of 7.5×10^4 cm^2/V s at room temperature and 1.5×10^5 cm^2/V s at low temperature. These values represent an approximately tenfold increase over those of our SiO$_2$-gated FLG as well as single and few-layer graphene reported in the literature, where μ ranges 2×10^3–2×10^4 cm^2/V s with weak or no temperature dependence [6,7,10,19]. This remarkable mobility improvement clearly demonstrates the advantage of the PZT substrate over SiO$_2$ towards fabricating graphene-based high-quality 2D systems. We note that Ref. [25]

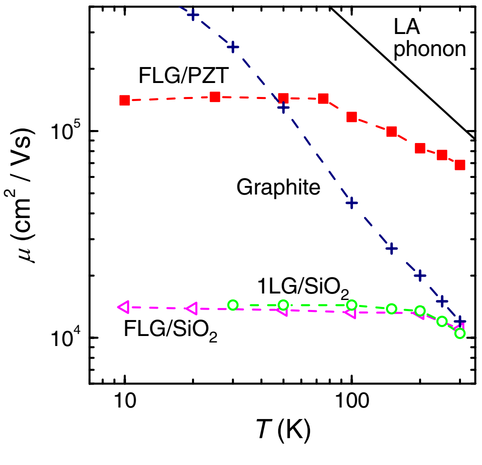

FIG. 4 (color online). Comparison of $\mu(T)$ in various graphitic materials. Solid squares: PZT-gated FLG shown in Fig. 3 at $n = 2.4 \times 10^{12}/\mathrm{cm}^2$. Open triangles: a SiO$_2$-gated FLG of the same thickness and density [17]. Open circles: single-layer graphene on SiO$_2$ reported in Ref. [10]. Crosses: mobility of bulk graphite from Ref. [21]. Solid line: LA phonon-limited mobility calculated from Eq. (4).

reports mobilities up to $6 \times 10^4\ \mathrm{cm^2/V\,s}$ at 4 K in thick multilayer graphene prepared on SiO_2, possibly due to their increasing 3D characteristics and reduced interactions with external scattering sources. Such samples exhibit $\mu < 1.5 \times 10^4\ \mathrm{cm^2/V\,s}$ at 300 K [25] compared to $\mu \sim 7 \times 10^4\ \mathrm{cm^2/V\,s}$ observed here.

The low-temperature residual mobility $\mu_0(n)$ in PZT-gated FLG exhibits a density dependence best described by $\mu_0(n) \sim n^{1.3}$ for $1.9 \times 10^{12}/\mathrm{cm}^2 < n < 2.4 \times 10^{12}/\mathrm{cm}^2$. In the inset of Fig. 3, we show $\mu_0(n)$ data in this range together with the fitting obtained in regime I: $\mu_0(n) \sim n^{0.9}$. This n-dependence of μ is in contrast to the SiO_2-gated graphene, where the scattering due to Coulomb impurities leads to a very weak n-dependence in a comparable density range, suggesting that different scattering mechanisms may be at work [2–7,19,26,27].

It has been shown in suspended graphene that a significant improvement in μ is only achieved after current annealing, which highlights the important role played by interfacial adsorbates [12], among other possible sources of scattering [7–10,28]. Our PZT substrates possess a large spontaneous polarization P pointing into the surface [17]. The absence of free carriers in ungated FLG devices indicates that this polarization is almost completely screened by a high-density layer of surface adsorbates prior to exfoliation. Screening adsorbates may come from free ions, atoms, and molecules in the ambient and OH^- and H^+ produced by the dissociation of H_2O on PZT surface [29,30]. Despite their high density, our data suggest that the scattering from interfacial adsorbates is much weaker than in SiO_2-gated devices. We attribute this remarkable phenomenon to the strong screening of PZT and speculate that some degree of ordering in the adsorbate layer may also play a role in reducing the scattering.

In conclusion, we have demonstrated a significant performance improvement in few-layer graphene FETs by using the crystalline ferroelectric gate oxide PZT. This approach has led us to the observation of the highest reported mobility to date in unsuspended single- and few-layer graphene devices. This result opens up a new route for realizing high-speed electronic devices and exploring novel 2D physics in graphene.

We are grateful to V. Crespi, P. Eklund, V. Henrich, J. Jain, P. Lammert, G. Mahan, J. Reiner, H. Stormer, and F. Walker for helpful discussions and E. Henriksen and M. Han for technical assistance. Work at Penn State is supported by NSF NIRT No. ECS-0609243 and NSF CAREER No. DMR-0748604. Fabrication of samples at Yale is supported by NSF MRSEC No. DMR-0520495, NSF No. DMR-0705799, ONR, and NRI. The authors also acknowledge use of NSF NNIN facilities at PSU.

---

[1] E. H. Hwang and S. Das Sarma, Phys. Rev. B **77**, 115449 (2008).
[2] T. Ando, J. Phys. Soc. Jpn. **75**, 074716 (2006).
[3] A. K. Geim and K. S. Novoselov, Nature Mater. **6**, 183 (2007).
[4] K. Nomura and A. H. MacDonald, Phys. Rev. Lett. **98**, 076602 (2007).
[5] E. H. Hwang, S. Adam, and S. Das Sarma, Phys. Rev. Lett. **98**, 186806 (2007).
[6] Y. W. Tan, Y. Zhang, K. Bolotin, Y. Zhao, S. Adam, E. H. Hwang, S. Das Sarma, H. L. Stormer, and P. Kim, Phys. Rev. Lett. **99**, 246803 (2007).
[7] S. V. Morozov, K. S. Novoselov, M. I. Katsnelson, F. Schedin, D. C. Elias, J. A. Jaszczak, and A. K. Geim, Phys. Rev. Lett. **100**, 016602 (2008).
[8] M. I. Katsnelson and A. K. Geim, Phil. Trans. R. Soc. A **366**, 195 (2008).
[9] S. Fratini and F. Guinea, Phys. Rev. B **77**, 195415 (2008).
[10] J.-H. Chen, C. Jang, S. Xiao, M. Ishigami, and M. S. Fuhrer, Nature Nanotech. **3**, 206 (2008).
[11] C. Jang, S. Adam, J.-H. Chen, E. D. Williams, S. DasSarma, and M. S. Fuhrer, Phys. Rev. Lett. **101**, 146805 (2008).
[12] K. I. Bolotin, K. J. Sikes, J. Hone, H. L. Stormer, and P. Kim, Phys. Rev. Lett. **101**, 096802 (2008).
[13] X. Du, I. Skachko, A. Barker, and E. Andrei, Nature Nanotech. **3**, 491 (2008).
[14] T. M. Mohiuddin, L. A. Ponomarenko, R. Yang, S. M. Morozov, A. A. Zhukov, F. Schedin, E. W. Hill, K. S. Novoselov, M. I. Katsnelson, and A. K. Geim, arXiv:0809.1162.
[15] S. Das Sarma, A. K. Geim, P. Kim, and A. H. MacDonald, Solid State Commun. **143**, 1 (2007).
[16] X. Hong, A. Posadas, A. Lin, and C. Ahn, Phys. Rev. B **68**, 134415 (2003).
[17] See EPAPS Document No. E-PRLTAO-102-013917 for supplementary details. For more information on EPAPS, see http://www.aip.org/pubservs/epaps.html.
[18] The charge neutrality point shifts to positive V_g ($\sim$2 V at 10 K) due to a slight increase of the polarization of the PZT film with decreasing temperature.
[19] K. Novoselov, A. Geim, S. Morozov, D. Jiang, Y. Zhang, S. Dubonos, I. Grigorieva, and A. Firsov, Science **306**, 666 (2004).
[20] B. Partoens and F. M. Peeters, Phys. Rev. B **74**, 075404 (2006).
[21] S. Ono and K. Sugihara, J. Phys. Soc. Jpn. **21**, 861 (1966).
[22] L. Yang, M. Anantram, J. Han, and J. Lu, Phys. Rev. B **60**, 13874 (1999).
[23] L. Woods and G. Mahan, Phys. Rev. B **61**, 10651 (2000).
[24] X. Du, S. Tsai, D. Maslov, and A. Hebard, Phys. Rev. Lett. **94**, 166601 (2005).
[25] S. V. Morozov, K. S. Novoselov, F. Schedin, D. Jiang, A. A. Firsov, and A. K. Geim, Phys. Rev. B **72**, 201401 (R) (2005).
[26] P. Price, Surf. Sci. **143**, 145 (1984).
[27] L. Pfeiffer, K. West, H. Stormer, and K. Baldwin, Appl. Phys. Lett. **55**, 1888 (1989).
[28] J. Martin, N. Akerman, G. Ulbricht, T. Lohmann, J. H. Smet, K. Von Klitzing, and A. Yacoby, Nature Phys. **4**, 144 (2008).
[29] F. Peter, K. Szot, R. Waser, B. Reichenberg, S. Tiedke, and J. Szade, Appl. Phys. Lett. **85**, 2896 (2004).
[30] M. Henderson, Surf. Sci. Rep. **46**, 5 (2002).